Electrochimica Acta 161 (2015) 403–407

Contents lists available at ScienceDirect

Electrochimica Acta

journal homepage: www.elsevier.com/locate/electacta

Individual thermoelectric properties of electrodeposited bismuth telluride nanowires in polycarbonate membranes

Taehoo Chang [a,1], Sungmee Cho [a,1], Jeongmin Kim [a], Jonathan Schoenleber [b], Cedric Frantz [b], Nicolas Stein [b,**], Clotilde Boulanger [b], Wooyoung Lee [a,*]

[a] Dept of Materials Science and Engineering, Yonsei University, 262 Seongsanno Seodaemun-gu, Seoul 129-749, South Korea
[b] Institut Jean Lamour, UMR 7198CNRS, University of Lorraine 1, bd Arago CP 87811, 57078 Metz Cedex 3, France

ARTICLE INFO

Article history:
Received 21 November 2014
Received in revised form 6 February 2015
Accepted 12 February 2015
Available online 14 February 2015

Keywords:
BiTe Nanowires
Polycarbonate membranes (PCM)
Thermoelectric (TE) property
Grain size

ABSTRACT

In this study, we examined individual bismuth telluride nanowires (NWs) electrodeposited in polycarbonate membranes (PCM) used as sacrificial templates. It has been demonstrated that the composition of Bi_2Te_3 is controlled by the electrodeposition conditions, e.g. the applied potential. High-resolution transmission electron microscopy (HRTEM) shows that the average grain size of NWs increases with increasing Te content. Our results also reveal that the electrodeposited bismuth telluride NWs are *n*-type, and their electrical conductivity increases with increasing Te content. These NWs also demonstrated a maximum power factor of 195.8 mW/m·K^2 for the Te-rich NW (d = 162 nm) at 300 K.

1. INTRODUCTION

Thermoelectricity is the phenomenon which results from the conversion of heat into electrical energy (Seebeck effect) or vice versa (Peltier effect). These materials offer a number of advantages, including high durability, no emission of toxic gases, and high reliability. They are suitable for a wide range of applications at various temperature regimes, such as power generation, refrigeration, sensing, and solid-state cooling [1]. On the other hand, the widespread use of thermoelectric (TE) materials has been restricted by their relatively low energy-conversion efficiency. Many efforts to improve their efficiency have focused entirely on improving the thermoelectric figure of merit, ZT, defined as $ZT = S^2\sigma T/(\kappa_l + \kappa_e)$, where S is the Seebeck coefficient, σ is the electrical conductivity, T is the absolute temperature, and κ_l and κ_e are the lattice and the electronic thermal conductivities respectively.

Among TE materials, bismuth telluride (Bi_2Te_3) and related alloys have proven to be among the most promising thermoelectric materials at room temperature ($ZT \approx 1.0$). These alloys are particularly attractive because they can be fabricated as *n*- or *p*-type TE materials by slightly varying their composition [2,3]. Generating nanostructures with low dimensionality is necessary for raising the electronic density of states closer to the Fermi level, increasing surface phonon scattering, and modifying phonon dispersion so as to improve values of ZT and make Bi_2Te_3 more efficient as regards TE properties [4–6]. Previously, significant improvements of ZT values were reported for nanostructured bulk alloys [7], nanoinclusions [8], nanocomposites [9], and thin-film superlattices [10,11]. Moreover, many different growth techniques have been explored to produce Bi_2Te_3 materials, including vapor-phase techniques [12–13], on-film formation of nanowires (OFF–ON) [14–16], and electrochemical deposition [17–21].

For Bi_2Te_3 nanowires (NWs) grown by electrodeposition, a high density of NWs along with a small diameter is required for producing miniaturized TE devices. High-density Bi_2Te_3 NWs are predominantly synthesized by a number of template-assisted methods using track-etched membranes [20–22], diblock copolymers [23,24], or anodized aluminum oxide (AAO) templates [25,26]. Of these, AAO templates have found particularly widespread usage owing to the simplicity and flexibility of their fabrication methods. AAO templates have thus been used in electrodeposition not only to obtain dense arrays of parallel NWs, but also to yield high deposition rates. However, the high thermal conductivity of alumina matrices has been known to induce thermal leakages in the alumina template [27,28]. A key challenge is to synthesize the NWs in a template-assisted membrane with lower thermal conductivities. Such a polymer membrane provides suitable electrical, thermal, chemical, and mechanical properties in the electrodeposition method.

* Corresponding author.
** Corresponding author.
E-mail addresses: Nicolas.stein@univ-lorraine.fr (N. Stein), Wooyoung@yonsei.ac.kr (W. Lee).
[1] These authors contributed equally to this work.

http://dx.doi.org/10.1016/j.electacta.2015.02.105
0013-4686/

In this paper, we report on thermoelectric properties of potentiostatically deposited Bi_2Te_3 NWs in polymer membranes (polycarbonate). The pore diameter can be controlled by chemical etching whereas the Bi:Te ratio of the Bi_2Te_3 NW can be tuned during the electrodeposition by applying different potentials. The thermoelectric properties of non-stoichiometric *n*-type Bi_2Te_3 (Bi_xTe_{1-x}) NWs showed that the NW electrical conductivity increases when Te is in excess in the deposit, and leads to an increase of the power factor at elevated temperatures.

2. EXPERIMENTAL

2.1. Template preparation

Polycarbonate membranes (PCMs) were used as templates to synthesize Bi_2Te_3 NWs. Polycarbonate foils (PCF, ~30 μm) were first irradiated using accelerated gold ions (energy ~2 GeV, fluence = 10^8 ions/cm^2) at the heavy ion accelerator UNILAC at the GSI Helmholtz Centre (Darmstadt, Germany). The resulting ion tracks were then sensitized by a 1 h UV exposure before being selectively dissolved and enlarged to make pores in a 6 N caustic soda solution (NaOH, Carlo Erba Reagents, 97%) at 50 °C. The resultant membranes contained pores of approximately 30, 60, and 120 nm in diameter, which were produced at a rate of 30 nm/min [29]. Following the etching process, a layer of platinum (~160 nm thick) was deposited by sputter deposition (Polaron SC7620) on one side of the PCFs to serve as a working electrode.

2.2. Electrochemical deposition

First Tellurium (Prolabo, 99.7%) was oxidized to $HTeO_2^+$ in 7 M HNO_3 (Carlo Erba Reagents, 65%) before adding $Bi(NO_3)_3$, $10H_2O$ (Fluka, >98%), deionized water (15MΩ) and then dimethyl sulfoxide (DMSO, Fisher Scientific, >99.9%). The quantities were adjusted to obtain the following concentrations in the electrolyte: 10 mM $HTeO_2^+$, 15 mM Bi^{3+}, 1 M HNO_3 and 50 v/v % DMSO. Before each experiment, dissolved oxygen was removed from the solutions by degassing with an argon flux for 20 min. Bi_2Te_3 was grown using a potentiostat (Autolab PGSTAT302) between −75 to −100 mV at room temperature (RT) with a three-electrode (Pt on PCM, Pt disc, and sat. Ag/AgCl reference) configuration. A more detailed description of this setup can be found elsewhere [20].

2.3. Device fabrication

Bi_2Te_3 NWs were first released from the template by dissolving the PCM in Dimethylformamid (DMF). The NWS, thereby suspended in DMF, were then collected by drop casting onto a thermally oxidized Si (500 nm SiO_2) substrate presenting alignment marks. All electrodes and micro-heaters were patterned using electron-beam (e-beam) lithography (VEGA 3 LM, Tescan Korea). The contact regions on the NWs were then etched by Ar plasma to remove their native oxide layers. For electrodes, chromium/gold (5-nm/250-nm thickness) films were deposited *in situ* via ultra-high vacuum (UHV) direct current (DC) magnetron sputtering at a base pressure of 4×10^{-8} Torr to prevent oxidation. A lift-off process was then used to remove the resist and release the nanowire device.

2.4. Characterization

After removal of the PCM templates, the microstructures and nanostructures of the Bi_2Te_3 NWs were characterized by transmission electron microscopy (TEM, Philips CM200) with energy-dispersive X-rays (EDX, X Max Oxford). Both the NW arrays and the fabricated devices were observed using scanning electron microscopy (SEM, ZEOL 7001 F). Thermoelectric property measurements were performed in a helium cryostat system in the temperature range 100–300 K. Measurements of Seebeck coefficients were conducted via two thermometers, with $S = \Delta V/\Delta T$, where ΔT is the temperature gradient across the NW, and ΔV is the Seebeck voltage generated by ΔT. ΔT was obtained by measuring the resistance of each thermometer with a lock-in amplifier (SR850, USA) whereas the voltage difference between the two thermometers was measured by a nanovoltmeter. The conductivity of the NWs was obtained using 4-probe measurement technique to remove contact resistance.

3. RESULTS AND DISCUSSION

Fig. 1 shows a typical current transient curve recorded during the potentiostatic deposition of Bi_2Te_3 NWs along with schematic views of the different steps during the PCM filling. After an initial nucleation (regime 1), the deposition current stabilizes to a steady-state value (regime 2). Nucleation occurs during the first stage, where current is controlled by charge transfer. The second stage corresponds to the growth process governed by diffusion mass transport [20]. Once the pores are filled (regime 3), the cathodic current increases sharply with the increase of the active surface area due to the NW outgrowths on the template surface. NWs were synthesized at both −75 mV and −100 mV in porous templates of various pore sizes based on our previous work [20].

Fig. 2 presents TEM images of Bi_2Te_3 NWs deposited at −75 mV and −100 mV in PCM templates. The diameter for both types of non-stoichiometric Bi_2Te_3 (Bi_xTe_{1-x}) NWs was ~60 nm. An enrichment of bismuth was observed with increasing cathodic potential. These observations are in agreement with previous results on electroplated films and can be explained by a larger overpotential which is favorable to the co-deposition of Bi^0 [20]. Selected area electron diffraction (SAED) patterns (insets in Fig. 2) are consistent with a polycrystalline state, which exhibit a preferential growth perpendicular to the (015) plane. These patterns display individual spots with small circular-arc shapes, which correspond to a weak disorientation around the zone axis of the analyzed grains.

To further observe the microstructure across the NWs, high-resolution TEM (HRTEM) was conducted, as shown in Fig. 3. The micrographs of both $Bi_{0.392}Te_{0.608}$ and $Bi_{0.442}Te_{0.558}$ NWs show a clear difference in grain sizes (average size of ~9.94 nm and

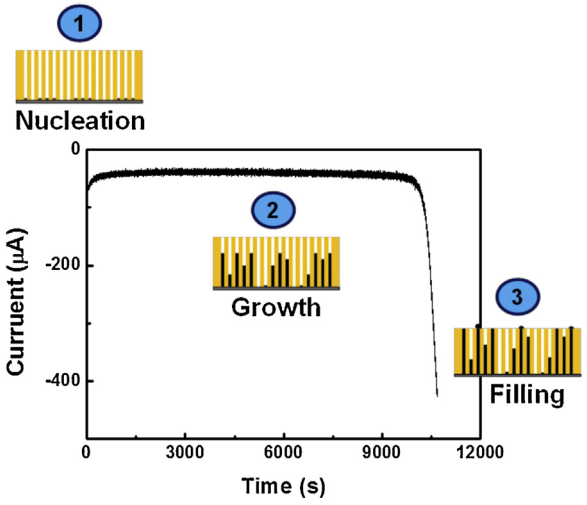

Fig. 1. A schematic of typical chronoamperometric response for Bi_xTe_{1-x} electrodeposition at −100 mV/sat. Ag/AgCl inside ion track etched polycarbonate membrane.

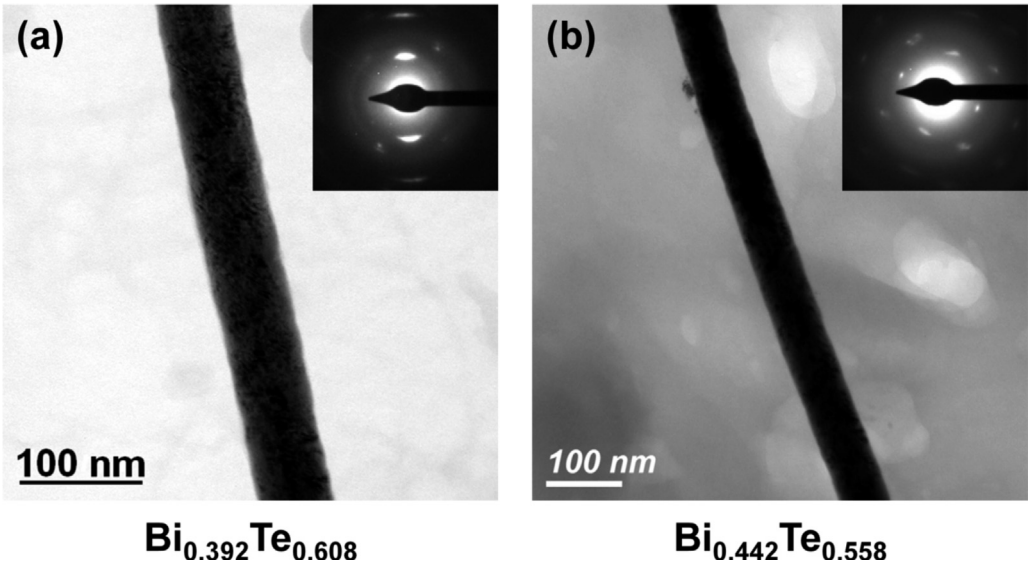

Fig. 2. TEM images of Bi_xTe_{1-x} NW deposited at (a) −75 mV and (b) −100 mV in PCM templates with 60 nm pore size. The inset is selected area electron diffraction (SAED) pattern.

~5.07 nm for $Bi_{0.392}Te_{0.608}$ and $Bi_{0.442}Te_{0.558}$, respectively) for NWs deposited at different potentials. The average grain size of non-stoichiometric Bi_2Te_3 NWs thus appeared to increase with increasing Te content, indicating that the electrodeposition potential does not only influence on doping extent but also on grain size in bismuth telluride NWs.

Fig. 4 shows a SEM image of a typical 4-probe device configuration (a) used to characterize the thermoelectric properties of individual bismuth telluride NWs, including the electrical conductivity (b), the Seebeck coefficient (c), and the calculated power factor (d). This device is composed of two sets of both thermometers (thermometer 1and 2) and leads (lead 1 and 2), and heater. The TE measurements were performed for as-deposited non-stoichiometric bismuth telluride NWs with different diameters (39, 71, 85, and 162 nm) in a temperature range from 100 K to 300 K. The TE measurements were conducted by the 4-terminal method to remove the contribution of contact resistance.

Electrical conductivity as a function of NW size (shown in Fig. 4(b)), which was used to calculate the thermoelectric power (TEP), is given by $S = (\sigma_e S_e + \sigma_h S_h)/(\sigma_e + \sigma_h)$, where the e and h conductivities of σ refer to electrons and holes, respectively. The more Te-rich NWs (red square, x = 0.39, d = 162 nm; orange diamond, x = 0.392, d = 71 nm, in Fig. 4) show degenerate conduction, owing to a significant contribution of added Te to carrier concentration [19]. On the other hand, the Bi-rich NWs (blue up triangle, x = 0.442, d = 85 nm; green down triangle, x = 0.42, d = 39 nm, in Fig. 4) exhibit semiconducting behavior, as proven by the increase of the electrical conductivity with the temperature. The complex temperature dependence of the electrical conductivity of bismuth telluride compounds has been already seen in the film or bulk form by changing synthesis conditions or relative content between Bi and Te [19]. In the nanowire structure, since the intrinsic properties such as carrier concentration, mobility, and effective mass cannot be obtained directly due to the limitation of quasi-one-dimensional structure, the typical Hall measurement cannot be employed to measure the intrinsic properties. Hence, to analyze the measured transport properties, the reported values of carrier concentration and mobility obtained from thin films were

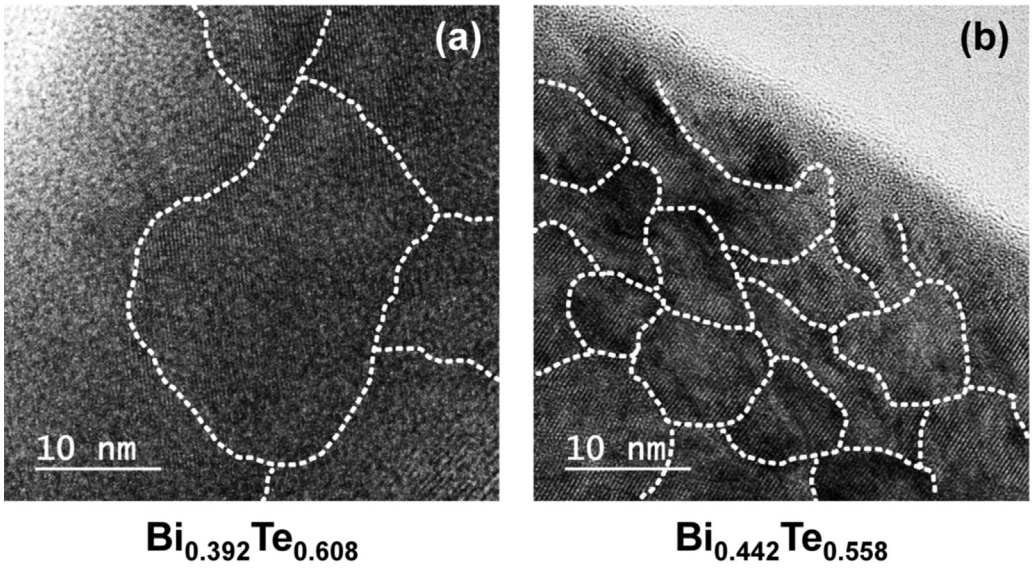

Fig. 3. HRTEM images for observing grain boundaries of Bi_xTe_{1-x} NW deposited at (a) −75 mV and (b) −100 mV.

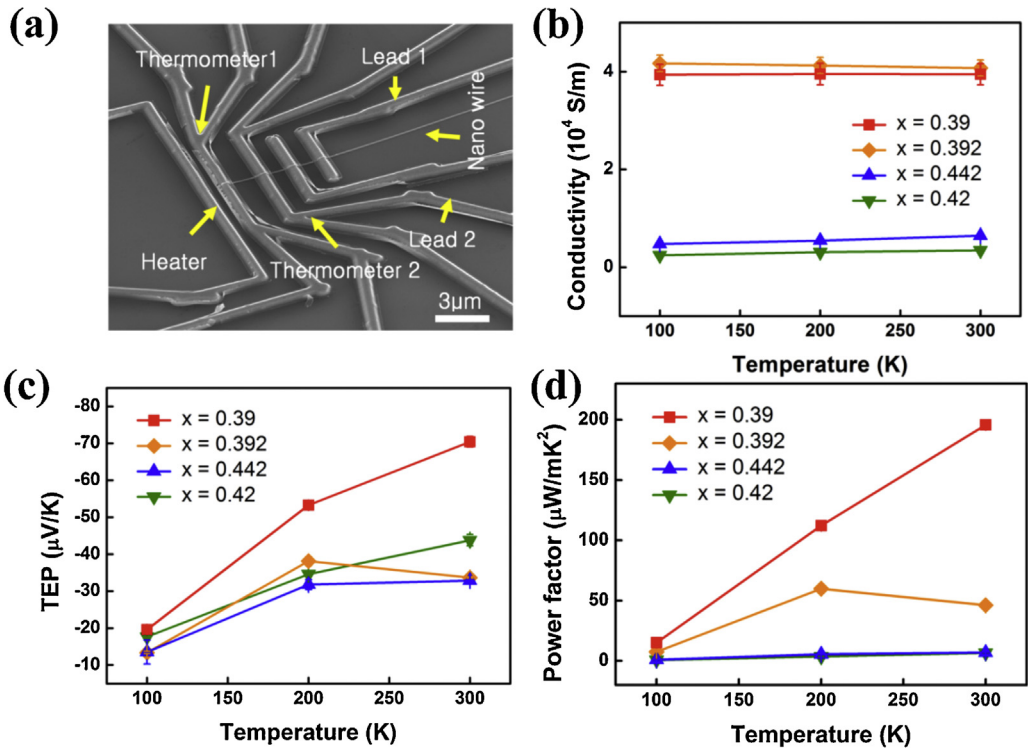

Fig. 4. (a) SEM image of a thermoelectric measurement device and measurement data for individual Bi_xTe_{1-x} nanowires: (b) electrical conductivity, (c) thermoelectric power, and (d) calculated power factor of individual nanowire as a function of temperature.

used. For Bi_xTe_{1-x}, the carrier concentration and mobility have been found to be about 5×10^{20} cm^{-3} at $0.39 < x < 0.392$ [30]. From this value, the carrier mobility of Te-rich NWs were calculated to be 5.01 ± 0.11 cm^2/Vs, which was half of the reported carrier mobility (~ 10 cm^2/Vs), indicating that the reduction of the carrier mobility can be attributed to surface scattering [18]. On the other hand, in the case of Bi-rich NWs ($0.44 < x < 0.42$), the carrier concentration was reported approximately 5×10^{19} cm^{-3}, which was a half value of Te-rich case [31]. In this case, the calculated carrier mobility was 6.07 ± 2.63 cm^2/Vs. It is noted that the estimated carrier mobilities of both Te- and Bi-rich NWs are comparable, indicating that the electrical conductivity was dominantly determined by the carrier concentration owing to the surface scattering dominated electron mean free path [18]. Accordingly, this reflects the fact that the temperature dependence of the electrical conductivity is also negligible from 100 K to 300 K [18]. Overall, it was found that the electrical conductivity of Te-rich NWs was about four times higher than that of Bi-rich NWs at all temperatures, which also appears to be related to the grain size of Bi_2Te_3 NWs, based on HRTEM observations (Fig. 3). The electrical conductivity at 300 K is around 4000 S/m for $Bi_{1.95}Te_{3.05}$ and $Bi_{1.96}Te_{3.04}$ samples, which is close to the bulk (5260 S/m) [32]. This result reflects the competition between semiconducting and semi-metallic character of bismuth telluride compounds depending to the stoichiometry [19]. The obtained TEP values, as shown in Fig. 4(c), were negative, indicating electrons as the majority charge carriers (n-type), although the average composition corresponds to a p-type semiconductor (Te content below 62 at.%) [3]; this can be explained by impurities or electrically active defects in the NWs [33]. The results are in good agreement with those of Mavrokefalos et al. [31], showing Seebeck coefficients of individual nanowires (Dia. #50 nm) between −50 and −70 μV/K at 300 K for polycrystalline and single crystalline states. In the investigated temperature range, the TEP absolute values increase linearly with increasing temperature for the Te-rich nanowires. At 300 K, the TEP of the Te-rich NW (orange, d = 71 nm, in Fig. 4(c)) exhibits a decline. Fig. 4(d) shows the thermoelectric power factor (σ^2S) of the non-stoichiometric bismuth telluride NWs at 100–300 K. The power factor for the Te-rich NW (red, d = 162 nm, in Fig. 4(d)) increases considerably with increasing temperature, with a maximum value of 195.8 μW/m·K^2 at 300 K; the power factor values of the Bi-rich NWs show a small increase from 100 K to 300 K. This value is in the same order of magnitude than those of electroplated films [33,34]. However the PF of the nanowires are still lower than the bulk (PF= 2560 μW/mK^2) [35] due to low Seebeck coefficients. Different reasons can explain these observations like the low doping concentration [36] or the low crystallographic quality leading to higher charge carrier concentration. Recently the group of K. Nielsch [37] suggests that thermoelectric transport of Bi_2Te_3 NWs can be reduced due to the strong influence of the surface, due to topological insulator behavior [38].

4. CONCLUSION

Bismuth telluride nanowires (NWs) were grown in polycarbonate membranes (PCMs) by potentiostatic electrodeposition. By applying two different potentials (−75 mV and −100 mV) during the electrodeposition, the ratio of bismuth to tellurium in the compound proved to be adjustable. HRTEM images show that the average grain sizes of both $Bi_{1.96}Te_{3.04}$ and $Bi_{2.21}Te_{2.79}$ NWs deposited at two different potentials of −75 mV and −100 mV were ~9.94 nm and ~5.07 nm, respectively. Our results indicate that non-stoichiometric Bi_2Te_3 NWs are *n*-type and the electrical conductivity was predominantly determined by the carrier concentration owing to the surface scattering dominated electron mean free path. The maximum power factor was obtained for the Te-rich NW (d = 162 nm) and was of 195.8 μW/m·K^2 at 300 K. This relatively high power factor mainly results from the increased electrical conductivity measured for Te-rich NWs.

ACKNOWLEDGEMENTS

This work was supported by the National Research Foundation of Korea (NRF) grant funded by the Korea government (MSIP) (2014R1A2A1A10053869), and the Priority Research Centers Program (2009-0093823) and the Pioneer Research Center Program (2013008070) through the NRF.

This work was also supported by the European Union "Fonds Européen de Développement Régional" n° 35962 and the Hubert Curien exchange program STAR 2011 n° 25853NF. The authors thank Dr. E. Toimil-Molares (GSI, Darmstadt, germany) for the ion-track irradiation.

References

[1] M. Zebarjadi, K. Esfarjani, M.S. Dresselhaus, Z.F. Ren, G. Chen, Energy & Environmental Science 1 (2012) 5147.
[2] G., Nolas, J., Sharp, H.J. Goldsmid, Eds. Thermoelectrics: Basic Principles and New Materials Developments, (SPRINGER, 2001).
[3] J.P. Fleurial, L. Gailliard, R. Triboulet, H. Scherrer, S. Scherrer, J. Phys. Chem. Solids 49 (1988) 1237.
[4] L.D. Hicks, M.S. Dresselhaus, Physical Review B 47 (1993) 12727.
[5] L.D. Hicks, M.S. Dresselhaus, Physical Review B 47 (1993) 16631.
[6] G. Chen, A. Shakouri, J. Heat Transfer 124 (2001) 242.
[7] A. Majumdar, Science 303 (2004) 777.
[8] F. Faleev, F. Leonard, Phys. Rev. B: Condens. Matter Mater. Phys 77 (2008) 14304.
[9] W. Xie, J. He, H.J. Kang, X. Tang, S. Zhu, M. Laver, S. Wang, J.R.D. Copley, C.M. Brown, Q. Zhang, T.M. Tritt, Nano Lett. 10 (2010) 3283.
[10] R. Venkatasubramanian, E. Siivola, T. Colptts, B. O'Quinn, Nature 413 (2001) 597.
[11] T.C. Harman, P.J. Taylor, M.P. Walsh, B.E. LaForge, Science 297 (2002) 2229.
[12] J. Heremans, C.M. Thrush, Physical Review B 59 (1999) 12579.
[13] S.B. Cronin, Y.M. Lin, T. Koga, X. Sun, J.Y. Ying, M.S. Dresselhaus, 18th International Conference on Thermoelectrics 554 (1999) .
[14] J. Ham, W. Shim, D.H. Kim, S. Lee, J. Roh, S.W. Sohn, K.H. Oh, P.W. Voorhees, W. Lee, Nano Lett. 9 (2009) 2867.
[15] J. Kang, J.W. Roh, W. Shim, J. Ham, J.-S. Noh, W. Lee, Adv. Mater 23 (2011) 3414.
[16] J. Kang, W. Shim, S. Lee, J.W. Roh, J.-S. Noh, P.W. Voorhees, W. Lee, J. Mater. Chem. A. 1 (2013) 2395.
[17] W. Wang, Q. Huang, F. Jia, J. Zhu, J. Appl. Phys. 96 (2004) 615.
[18] J. Zhou, C. Jin, J.H. Seol, X. Li, L. Shi, Appl. Phys. Lett. 87 (2005) 133109.
[19] C.L. Chen, Y.Y. Chen, S.J. Lin, C. Ho, P.C. Lee, C.D. Chen, S.R. Harutyunyan, J. Phys. Chem. C 114 (2010) 3385.
[20] C. Frantz, N. Stein, Y. Zhang, E. Bouzy, O. Picht, M.E. Toimil-Molares, C. Boulanger, Electrochimica Acta 69 (2012) 30–37.
[21] C. Frantz, N. Stein, L. Gravier, S. Granville, C. Boulanger, J. Electronic Materials 39 (2010) 2043.
[22] O. Picht, S. Mueller, I. Alber, M. Rauber, J. Lensch-Falk, D.L. Medlin, R. Neumann, M.E. Toimil-Molares, Physical Chemistry C 116 (2012) 5367.
[23] T. Thurn-Albrecht, J. Schotter, G.A. Kastle, N. Emley, T. Shibauchi, L. Krusin-Elbaum, G. Guarine, C.T. Black, M.T. Touminen, T.P. Russell, Science 290 (2000) 2126.
[24] M. Bal, A. Ursache, M.T. Tuominen, J.T. Goldbach, T.P. Russell, Appl. Phys. Lett. 81 (2002) 3479.
[25] J. Lee, Y. Kim, L. Cagnon, U. Gosele, J. Lee, K. Nielsch, Physica Status Solid-Rapid Research Letters 4 (2010) 43.
[26] A.L. Prieto, M.S. Sander, M.S. Martin-Gonzalez, R. Gronsky, T. Sands, A.M. Stacy, J. Am. Chem. Soc. 7160 (2001) 123.
[27] C.R. Martin, Science 266 (1994) 1961.
[28] M.B. Hariri, A. Dolati, R.S. Moakhar, J. Electrochem. Soc. 160 (2013) D279.
[29] T.W. Cornelius, P.Y. Apel, B. Schiedt, C. Trautmann, M.E. Toimil-Molares, S. Karim, R. Neumann, Nuclear Instruments & Methods in Physics Research Section B Beam Interactions with Materials and Atoms 265 (2007) 553.
[30] Y. Maa, E. Ahlberg, Y. Sun, B.B. Iversen, A.E.C. Palmqvist, Electrochimica Acta 56 (2011) 4216.
[31] A. Mavrokefalos, A.L. Moore, M.T. Pettes, L. Shi, W. Wang, X. Li, J. Applied Physics 105 (2009) 104318.
[32] D.M. Rowe, Handbook of thermoeletrics, 1995.
[33] B.Y. Yoo, C.K. Huang, J.R. Lim, J. Herman, M.A. Ryan, J.P. Fleurial, N.V. Myung, Electrochimica Acta 50 (2005) 4371.
[34] W.L. Wang, C.C. Wan, Y.Y. Wang, Electrochimica Acta 52 (2007) 6502.
[35] T. Yasue, H. Koyama, T. Kato, T. Nishioka, J. Vac. Sci. Technol. B 15 (1997) 614.
[36] S. Bassler, T. Bohnert, J. Gooth, C. Schumacher, E. Pippel, K. Nielsch, Nanotechnology 24 (2013) 495402.
[37] B. Hamdou, A. Beckstedt, J. Kimling, A. Dorn, L. Akinsinde, S. Bäßler, E. Pippel, K. Nielsch, Nanotechnology 25 (2014) 365401.
[38] B. Hamdou, J. Gooth, A. Dorn, E. Pippel, K. Nielsch, Applied Physics Letters 103 (2013) 193107.